Pure Appl. Opt. 4 (1995) 553–570. Printed in the UK

Binarization of continuous-tone pupil filters: a comparison of several digital halftoning procedures

Marek Kowalczyk†§, Tomasz Cichocki‡, Manuel Martínez-Corral‡‖ and Vitaly Kober‡¶

† Department of Optics, University of Valencia, 46100 Burjassot, Spain
‡ Institute of Geophysics, Warsaw University, Pasteura 7, 02093 Warsaw, Poland

Received 22 July 1994, in final form 21 February 1995

Abstract. Nine digital halftoning procedures, including two algorithms proposed by us, are compared to find out which one is best suited for binarization of continuous-tone pupil filters. The procedures we deal with include iterative, error diffusion, error convergence and one-pixel algorithms. In our numerical experiment the performance of binary filters is examined in terms of two parameters: the resemblance of their amplitude impulse response (AIR) to the AIR of the original continuous filter, as well as their light efficiency. The examination is carried on for super-resolving, apodizing and sine-wave pupil filters. The results are to a certain extent object dependent, nevertheless some general conclusions are presented.

1. Introduction

The performance of a linear coherent imaging system can be described by means of either its amplitude impulse response (AIR) or a Fourier transform of this magnitude, i.e. the coherent transfer function. In an optical experiment we can directly shape this coherent transfer function by placing a filter in the pupil plane of the system, and in this way we can control the AIR. The design of pupil-plane filters, for example apodizing filters, super-resolving filters, deblurring filters, etc, has been extensively studied [1, 2]. Nonetheless, the manufacturing of continuous-tone pupil filters has remained a difficult task. A possible solution to this difficulty is to fabricate pupil filters in the binary form by means of high resolution computer-controlled light plotters [3, 4]. The fact that the size of a binary element may be controlled more easily than the optical density of a thin film underlies the attractiveness of this idea. Therefore, the influence of the binarization procedure on the performance of a binary filter should be examined.

When binarization methods are used for creation of illusion of continuous-tone pictures (halftoning), the resulting binary image is usually examined both in the spatial domain and in the Fourier domain. In the spatial domain, subjective visual criteria are applied. In the Fourier domain, we examine isotropy, regularity and extension of the

§ Permanent address: Institute of Geophysics, Warsaw University, Pasteura 7, 02093 Warsaw, Poland.
‖ Permanent address: Department of Optics, University of Valencia, 46100 Burjassot, Spain.
¶ Permanent address: Institute of Information Transmission Problems, Russian Academy of Science, 19 Yermolovoy str., GSP-4, 101447 Moscow, Russia.

0963-9659/95/050553+18 $19.50

spectrum of a uniformly gray object rendered with a given halftoning method [5]. On the other hand, when binarization methods are used to implement the binary version of a diffractive optical element (DOE), e.g. a pupil filter, the performance of the binary mask is evaluated only in the spatial frequency domain, where the Fourier spectrum of its amplitude transmittance, that is, its amplitude impulse response (AIR), is compared with the Fourier spectrum of the original continuous-tone element.

A general analytic approach that enables us to predict how a binarization procedure affects the spectrum of a digitally halftoned object is available only for three classes of halftone procedures. The first class consists of all the techniques based on the periodic carrier concept [4–8]. The use of these methods would strongly affect the resemblance between the AIRs of binarized and continuous-tone pupil filters. This is because irrespective of the nature of the continuous-tone filter spectrum, the spectrum of the corresponding binary filter is periodic. Those techniques will therefore not be addressed here.

The second class consists of generalized deterministic error diffusion procedures (without stochastic perturbations [5]). A comprehensive analysis of the spectra of binarized images and DOE obtained by means of these algorithms was presented in terms of filter theory by Weissbach and Wyrowski [9].

The third class consists of procedures based on the random carrier concept. A technique which belongs to this class is, for example, that presented by Mitsa and Parker [10] in which the halftoning is achieved by a pixelwise comparison of gray scale image to a blue-noise mask. In recent work, we presented a rigorous analytic description of dithering with a white-noise mask [11]. We showed that the statistical average of the AIR of a pupil filter binarized with this method is approximately equal to the AIR of the corresponding continuous-tone filter provided that the number of transparent cells within the pupil is sufficiently large. Dithering with white noise has until now been a unique digital halftoning method with non-periodic carrier which is applicable to binarization of pupil filters.

The aim of this paper is to find a binarization method which would yield the spectra of a binary filter and its corresponding continuous-tone filter as similar as possible and at the same time would provide the light efficiency of the binary filter close to that of its continuous-tone counterpart. Since, in general, approximately 90% of the AIR energy is concentrated in its central maximum and low order side lobes, we are looking for a procedure which would not affect the low frequency part of the spectrum of the filter transmittance. There exist binarization methods whose actual implementation is well adapted to our needs. This favourable situation results from the fact that in order to meet the subjective criteria of human understanding of images, many halftone procedures have been optimized so as to give an isotropic blue-noise shape to the spectrum of binarization noise. The blue-noise spectrum of binarization noise means that the low frequency part of the spectrum of continuous tone element remains practically unaffected when the binarization procedure is executed which, by coincidence, is exactly our aim. The blue-noise shape of the spectrum is an inherent feature of all the error diffusion procedures, unless they are intentionally modified so as to provide another spectral distribution of the binarization noise [12]. The blue-noise shape of the binarization noise spectrum can also be achieved in some iterative halftone procedures in which the shape of a fixed part of the spectrum is directly controlled.

Since analytical description of the influence of digital halftoning on the Fourier spectrum is available only for deterministic error diffusion and for dithering with a random carrier, we perform here a numerical experiment to compare the performance

of the nine binary versions of the following pupil–plane filters:

- super-resolving parabolic filter
- apodizing parabolic filter
- sine-wave filter.

Each binary version is generated by a different halftoning algorithm. The use of the super-resolving and apodizing pupils as test objects in our numerical experiment seems obvious. The use of a sine-wave filter needs a comment. The great majority of real slowly-varying pupil functions possess at least two perpendicular axes of symmetry. Thus, the examination of the sine-wave pupil is of low practical interest. Nevertheless we do consider it because the lack of symmetry of this pupil may affect the results obtained with some algorithms that we test here. Binarization of a sine wave by means of digital halftoning was considered by Billotet-Hoffman and Bryngdahl but only qualitative results were presented [13].

We examine all of the binary filters for the resemblance of their spectra to that of the corresponding continuous-tone filter and for their light efficiency. We evaluate both parameters because for some binarization procedures there exists a trade-off between them and a binary filter whose spectrum very much resembles that of the continuous-tone filter may be found unacceptable due to its poor light efficiency. By the 'light efficiency' we mean here the fraction of incident light energy which is diffracted by a filter towards an arbitrary window of interest.

2. Description of the algorithms

A wide range of two-dimensional digital halftoning techniques which are good blue-noise generators has been reported in the literature [5]. Here we limit our interest to six of them, representing different approaches, and to two procedures which are proposed here. We also test the dithering with white noise, a unique procedure only recommended until now for the binarization of pupil filters. We consider it a reference point. In this way, we study the performance of the following binarization methods.

(a) Dithering with white noise [11].

(b) Error diffusion with a Floyd and Steinberg error filter [14].

(c) Error diffusion with one weight which is randomly positioned [5].

(d) Error diffusion with a Floyd and Steinberg filter perturbed by a uniformly distributed bipolar additive white noise [5].

(e) Error diffusion with the Floyd and Steinberg filter perturbed by a properly scaled output of symmetrical hardclipper with the noise generated in (d) used as the input.

(f) Multiresolution, error-convergence algorithm [15].

(g) Multiresolution, error-convergence algorithm with random choice of testing pixels [15].

(h) Modification of (f) by increasing the number of testing pixels.

(i) Iterative Fourier transform algorithm [16, 17].

The algorithms (a) and (b) are completely described in the literature whereas the algorithms (c), (d), (f), (g) and (i) contain some free parameters that should be specified. Finally, the algorithms (e) and (h) proposed here are modifications of (d) and (f), respectively. They were both intended to improve the performance of the original versions.

For the versions (c), (d) and (e) of the error diffusion method, the algorithms are processed pixel by pixel on a serpentine raster (see figure 1).

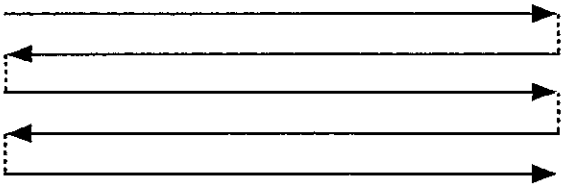

Figure 1. Serpentine raster path.

Figure 2. Two one-weight error filters used when the row of pixels is processed from left to right. We select with equal probability one of them to diffuse the error from the origin position marked '•'.

In the case of error diffusion with one randomly positioned weight (algorithm (c)), we select the position of the weight with equal probability between two candidate locations, immediately below and preceding the filter origin (figure 2).

In the case of error diffusion with the Floyd and Steinberg filter perturbed by white noise (algorithm (d)), we start by pairing original Floyd and Steinberg weights of comparable value. We form two pairs $(\frac{1}{16}, \frac{3}{16})$ and $(\frac{5}{16}, \frac{7}{16})$. Then for each pixel two statistically independent random variables χ and ψ are generated. The random variable χ perturbs the $(\frac{1}{16}, \frac{3}{16})$ pair and ψ the other one. These random variables have the following uniform probability density functions

$$p_\chi(\chi) = \begin{cases} 8 & -\frac{1}{16} \le \chi \le \frac{1}{16} \\ 0 & \text{otherwise} \end{cases} \tag{1}$$

and

$$p_\psi(\psi) = \begin{cases} 1.6 & -\frac{5}{16} \le \psi \le \frac{5}{16} \\ 0 & \text{otherwise.} \end{cases} \tag{2}$$

Next, we multiply χ and ψ by b and b', respectively, where b and b' belong to the [0, 1] interval. Then $b\chi$ and $b'\psi$ perturb the corresponding pairs:

$$(\tfrac{1}{16}, \tfrac{3}{16}) \to (\tfrac{1}{16} + b\chi, \tfrac{3}{16} - b\chi) \tag{3}$$

and

$$(\tfrac{5}{16}, \tfrac{7}{16}) \to (\tfrac{5}{16} + b'\psi, \tfrac{7}{16} - b'\psi). \tag{4}$$

The scaling factors b and b' express the maximum percentage of the smaller weight in the pair affected by noise. In our experiment $b = b' = 0.5$. Thus, in every sampled point of the filter we use the error-diffusion filter shown in figure 3.

$$\left(\frac{1}{16}\times\right) \begin{matrix} & & \bullet & 7-8\psi \\ 3-8\chi & 5+8\psi & 1+8\chi & \end{matrix}$$

Figure 3. Error filter used when the classical weights of Floyd and Steinberg are perturbed by a uniformly distributed bipolar additive white noise.

$$\left(\frac{1}{32}\times\right)\begin{array}{ccc} & \bullet & 19 \\ 5 & 5 & 3 \end{array} \qquad \left(\frac{1}{32}\times\right)\begin{array}{ccc} & \bullet & 19 \\ 7 & 5 & 1 \end{array}$$

$$\left(\frac{1}{32}\times\right)\begin{array}{ccc} & \bullet & 9 \\ 5 & 15 & 3 \end{array} \qquad \left(\frac{1}{32}\times\right)\begin{array}{ccc} & \bullet & 9 \\ 7 & 15 & 1 \end{array}$$

Figure 4. Error filters used in the algorithm (e) (for rows of pixels processed from left to right).

In our modification of the above binarization algorithm (that is, in algorithm (e)), the random variable χ can take, with equal probability, only two values $-\frac{1}{16}$ and $\frac{1}{16}$, whereas the variable ψ can take the values $-\frac{5}{15}$ and $\frac{5}{16}$. Again we assume that χ and ψ are statistically independent, so that at every point of the filter we use with equal probability one of the four error filters presented in figure 4.

The multiresolution, error-convergence halftone algorithm (algorithm (f)) can be considered as a parallel-processed symmetrical error-diffusion algorithm. Thus it is supposed to be free from directional hysteresis which is typical of all error diffusion methods processed sequentially. A distinctive feature of this algorithm is its pyramidal structure. At the first pyramid level, the original continuous-tone image is hardclipped pixel by pixel to produce the binary image. At higher levels the binarized image is compared with the continuous-tone image over a window of pixels for calculation of a weighted averaged error. The binary assignment is then changed if the weighted averaged error exceeds a threshold value that can be determined analytically or adjusted experimentally. During comparison we centre the window at the selected binarized pixels (see figure 2 in [14]). The theoretical and experimental threshold values do not coincide and they both depend on the pyramid level. The threshold values that we use in the algorithms (f), (g) and (h) are presented in table 1. The number and distribution of tested pixels and the size of the window depend on the pyramid level. In our calculation we use five pyramid levels and at each level we test a subset of the pixels and apply the windows proposed by Peli in the basic version of the algorithm [14].

The basic version of the multiresolution, error-convergence algorithm described above has the drawback that when it renders some gray levels it yields false contours and directional patterns (textures). To reduce these effects we follow Peli's idea of

Table 1. Error thresholds used to determine whether a pixel binary assignment should be changed.

	Pyramid level			
Algorithm	2	3	4	5
(f), (h)	43/255	14/255	9/255	7/255
(g)	64/255	36/255	10/255	3/255

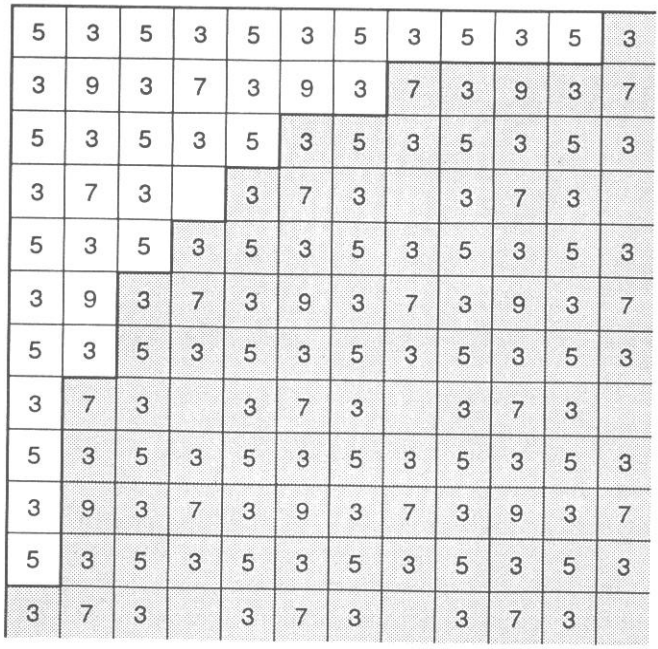

Figure 5. Pixels tested for possible change of binary assignment are marked with odd numbers $2n-1$ where n is the pyramid level and $(2n-1)\times(2n-1)$ is the size of the window used for calculation of the weighted average error. The shaded area corresponds to a quadrant of the clear pupil.

including pseudorandom noise in the choise of pixels to be tested at each pyramid level (algorithm (g)). In this case, the probability of shifting a tested point from its central position to any of eight neighbouring positions is given by the matrix

$$\mathbf{M} = \begin{bmatrix} \frac{1}{60} & \frac{2}{15} & \frac{1}{60} \\ \frac{1}{15} & \frac{8}{15} & \frac{1}{15} \\ \frac{1}{60} & \frac{2}{15} & \frac{1}{60} \end{bmatrix}. \tag{6}$$

It follows from equation (6) that the probability of the tested pixel being one of those which form the regular grid corresponding to a given pyramid level is equal to $\frac{8}{15}$. Thus, almost 50% of points supposed to be tested are randomly shifted from the positions they occupy in the deterministic version of the algorithm.

We propose here another attempt to improve the performance of algorithm (f). Our modification consists in duplication of the number of testing points and in a new distribution of them (algorithm (h)). The pixel positions that we test for change of binary assignment at all levels of the pyramid are shown in figure 5.

In the iterative Fourier transform algorithm (i) the binary transmittance is approached stepwise. We start with the continuous-tone transmittance $t(u, v)$ and execute the iterative procedure according to the flow-chart presented in figure 6. The operators $\mathscr{U}$ and $\mathscr{H}$ represent the constraints imposed on $t_j(u, v)$ and on the Fourier transform of

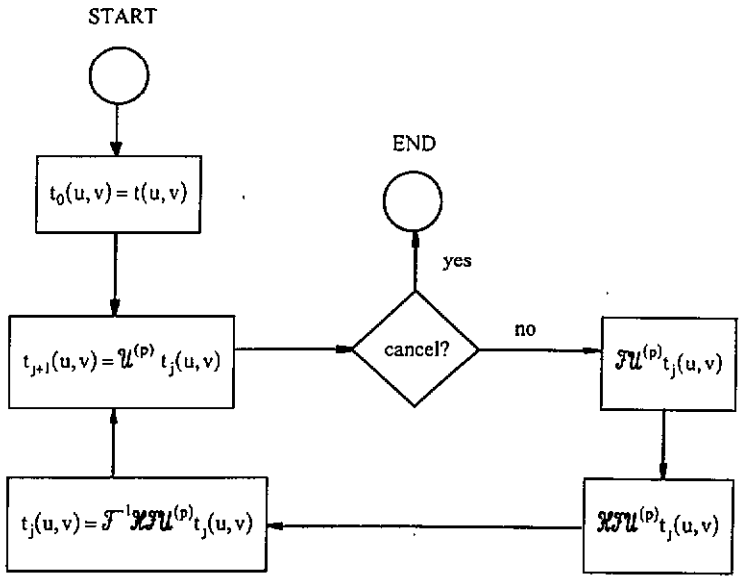

Figure 6. Flow chart for the iterative Fourier transform algorithm used to calculate binary filters.

$\mathcal{U}t_j(u, v)$, which we denote as $T_j(x, y)$. The operators are defined as follows

$$\mathcal{U}^{(p)}t_j(u,v) = \begin{cases} 0 & |t_j(u,v)| \le e^{(p)} \\ 1 & |t_j(u,v)| > 1 - e^{(p)} \\ |t_j(u,v)| & \text{otherwise} \end{cases} \qquad \begin{matrix} j = 0, 1, 2, \ldots, 549 \\ p = 0, 1, 2, \ldots, 46 \end{matrix} \tag{7}$$

and

$$\mathcal{H}T_j(x,y) = \begin{cases} \beta_j |T(x,y)| \exp\{i \arg[T_j(x,y)]\} & (x,y) \in S \\ T_j(x,y) & \text{otherwise} \end{cases} \tag{8}$$

where $T(x, y)$ is the Fourier transform of $t(u, v)$ and β_j is the proportionality constant that minimizes the quadratic deviation of T_j from T over the window S [17]. In the case of apodizing and super-resolving pupils the area S in which $T_j(x, y)$ is substituted by $\beta_j|T(x, y)| \exp\{i \arg[T_j(x, y)\}$ is a circle bounded by the second zero ring in $T(x, y)$. In the case of a sine-wave pupil the area S is a rectangle in the low-pass region whose sides are parallel to the x, y axes. It covers the main lobe and eight neighbouring side lobes of $T(x, y)$. The parameter $e^{(p)}$ increases by 0.01 every 10 iterations within the range 0.05–0.50. In order to evaluate the direct and inverse Fourier transform we use a fast Fourier transform (FFT). For this purpose binary filters, with diameter of 23 pixels (the case of rotationally symmetric $T(x, y)$) or with the size 32 × 32 pixels (the case of sine-wave filters) are placed in the 128 × 128 matrix of pixels.

Summarizing: procedure (a) has been chosen as a reference point. Algorithms (b)–(e) have nearly blue-noise characteristics. Algorithms (f)–(h) have a slightly poorer blue-noise spectrum and are more sensitive to edge effects, but on the other hand they are free from directional hysteresis. Finally, algorithm (i) has been chosen because it was designed to obtain a high degree of resemblance between the spectrum of a continuous-tone element and that of its binary version, what is just our aim here.

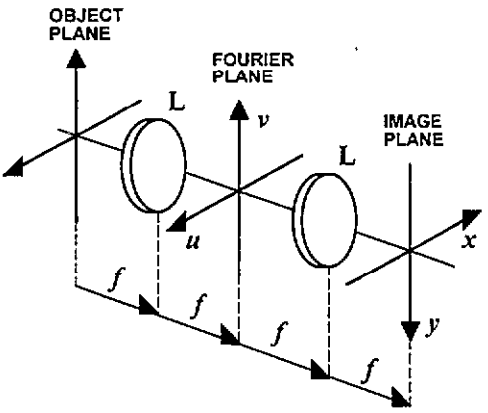

Figure 7. The configuration assumed in our numerical experiment; L, Fourier transform lenses.

3. Numerical experiment

In the first stage of our numerical experiment three sets of nine binary filters are generated on rectangular grids. These sets correspond to three continuous-tone pupil functions

$$t_1(u, v) = \operatorname{circ}\left(\frac{(u^2 + v^2)^{1/2}}{R}\right)\frac{u^2 + v^2}{R^2} \tag{9a}$$

$$t_2(u, v) = \operatorname{circ}\left(\frac{(u^2 + v^2)^{1/2}}{R}\right)\left(1 - \frac{u^2 + v^2}{R^2}\right) \tag{9b}$$

$$t_3(u, v) = \frac{1}{2}\left(\sin\frac{2\pi u}{L} + 1\right)\operatorname{rect}\frac{u}{L}\operatorname{rect}\frac{v}{L} \tag{9c}$$

where (u, v) are the spatial coordinates in the filter plane, R is the radius of the super-resolving and apodizing filters, and L is the size of the square sine-wave pupil. The coherent transfer function of the $4f$ imaging system with t_i filter in its Fourier plane (figure 7) is equal to

$$P_i(\mu, \eta) = t_i(\mu\lambda f, \eta\lambda f) \qquad i = 1, 2, 3 \tag{10}$$

where (μ, η) are the spatial frequency coordinates in the Fourier plane and λ is the wavelength of the coherent illuminating beam. The sets of filters obtained with algorithms (a)–(i) are shown in figures 8–10. It is seen that the only filters that preserve the symmetry of the clear pupil which is built with square cells (see the shaded area in figure 5) are those obtained with parallel processed deterministic algorithms ((f), (h) and (i)).

In the second stage we calculate the intensity distributions in the images of an axial point source obtained in the $4f$ imaging system with the subsequent binary filters in the Fourier plane. That is, we calculate the squared modulus of the AIR of each binary filter. The intensity distributions are shown in figures 11–13 where they are qualitatively compared with those obtained for the clear pupil and the continuous-tone filter.

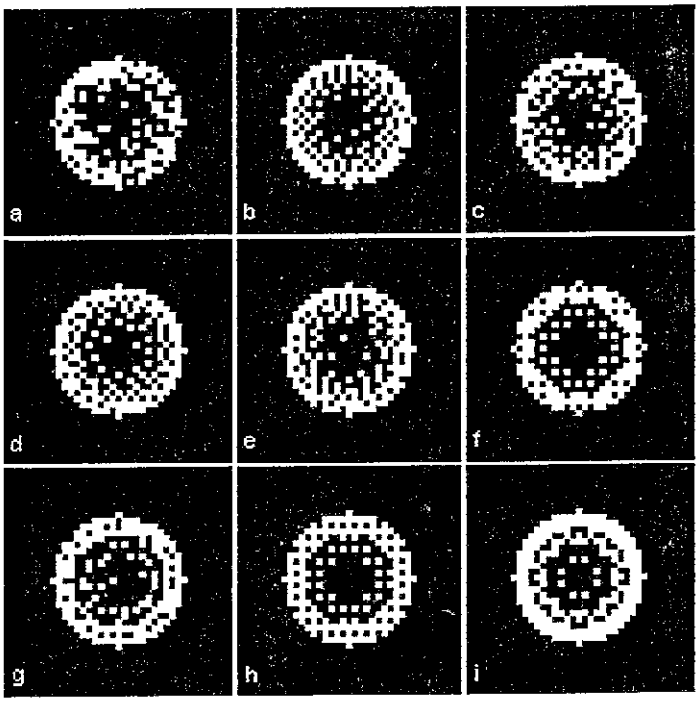

Figure 8. Super-resolving binary filters obtained with algorithms (a)–(i).

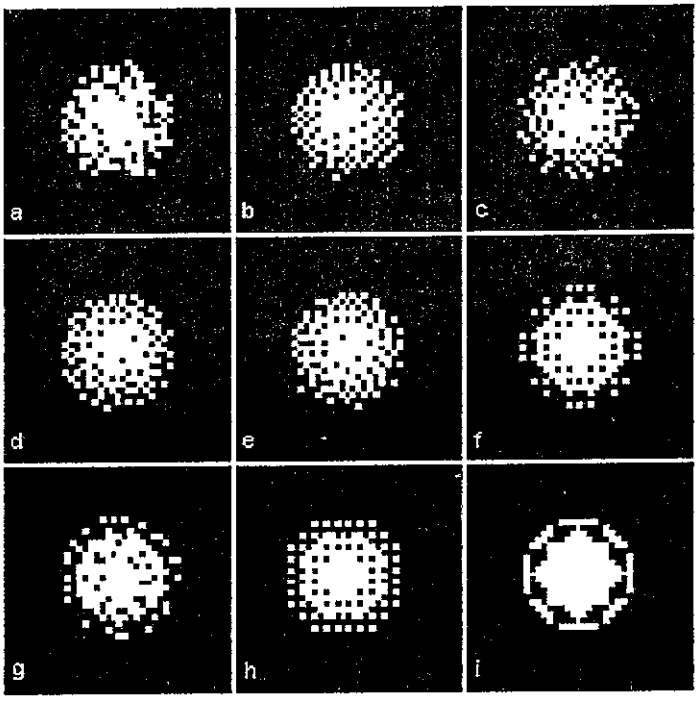

Figure 9. Apodizing binary filters obtained with algorithms (a)–(i).

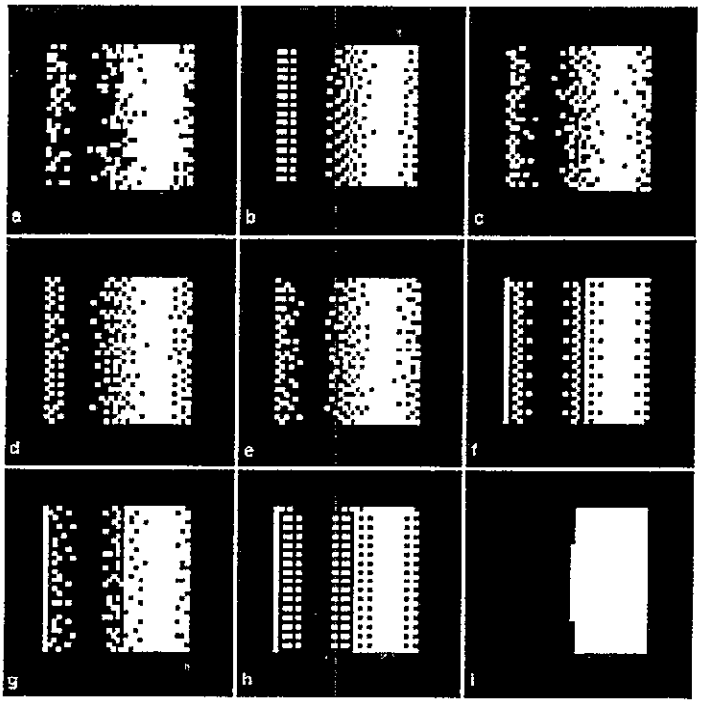

Figure 10. Sine-wave binary filters obtained with algorithms (a)–(i).

In order to evaluate the resemblance of the AIR of binary filters to the AIR of their continuous-tone counterparts, we use the signal-to-noise ratio (SNR) as proposed by Weissbach and Wyrowski [8]:

$$\text{SNR} = \frac{\int\int_A [F(x, y)]^2 \, dx \, dy}{\int\int_A [F(x, y) - \alpha G(x, y)]^2 \, dx \, dy} \tag{11}$$

where coefficient

$$\alpha = \frac{\int\int_A F(x, y) G(x, y) \, dx \, dy}{\int\int_A [G(x, y)]^2 \, dx \, dy} \tag{12}$$

maximizes the SNR. In our calculations $F(x, y)$ stands for the squared modulus of the AIR of the continuous-tone filter and $G(x, y)$ stands for $|\text{AIR}|^2$ of the binary one. In the case of super-resolving and apodizing filters the square area A is centred at the optical axis and its side is equal to the diameter of the second zero ring of $T(x, y)$. In the case of sine-wave filters the rectangular area A covers the main lobe and the first-order side lobes of $T(x, y)$, i.e. it coincides with the area S. The AIR of binary filters are calculated with FFT, where the size of filters and the size of matrix of pixels are the same as we use in the iterative Fourier transform algorithm. We use the SNR defined in equations (11) and (12) as a merit function which orders all the algorithms according to the degree of resemblance between the AIR of the corresponding binary filters and that of the continuous one.

The values of the SNR are presented in table 2. For algorithms that use random number generators ((a), (c), (d), (e) and (g)), in fact we generate ensembles that consist

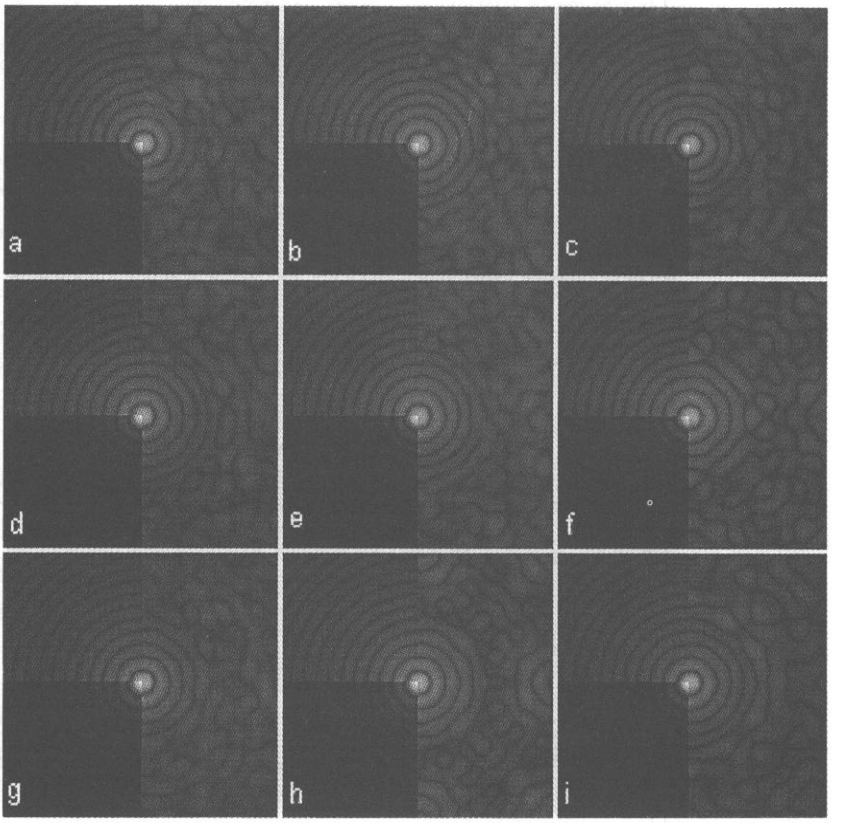

Figure 11. Squared moduli of the AIR of super-resolving binary filters obtained with algorithms (a)–(i). In the upper left quadrants $|\text{AIR}|^2$ of the continuous-tone filter is shown. In order to demonstrate the super-resolving properties of binary filters the $|\text{AIR}|^2$ of the clear pupil is shown in the lower left quadrants.

of 100 sample filters. In table 2 we show the SNR of the best samples selected from the ensembles, which are exactly the samples shown in figures 8–10. In table 2 we also present the average signal-to-noise ratio, $\overline{\text{SNR}}$, and the standard deviation of SNR, σ_{SNR}, that characterize the entire ensembles. In the case of the sine-wave filter we present two values of the corresponding parameters for error-diffusion algorithms. The upper value is obtained when the lines of the serpentine raster (the full lines in figure 1) are perpendicular to the fringes of sine-wave transmittance. The lower values (in parentheses) correspond to the parallel direction of execution of error-diffusion algorithms.

A quantitative graphical comparison of the AIR of binary filters and those of their gray-tone counterparts is presented in figure 14, where their cross sections are plotted for the best and the worst (as regards the SNR) super-resolving, apodizing and sine-wave filters. It is evident that within the window A the distributions $\alpha G(c, y)$ coincide almost perfectly with $F(x, y)$. Therefore α^{-1} can be considered the light efficiency of the binary pupil filter related to the light efficiency of the underlying gray-tone filter. The values of α^{-1}, too, are presented in table 2. All of them are close to unity:

$$0.783 \leq \alpha^{-1} \leq 1.294. \tag{13}$$

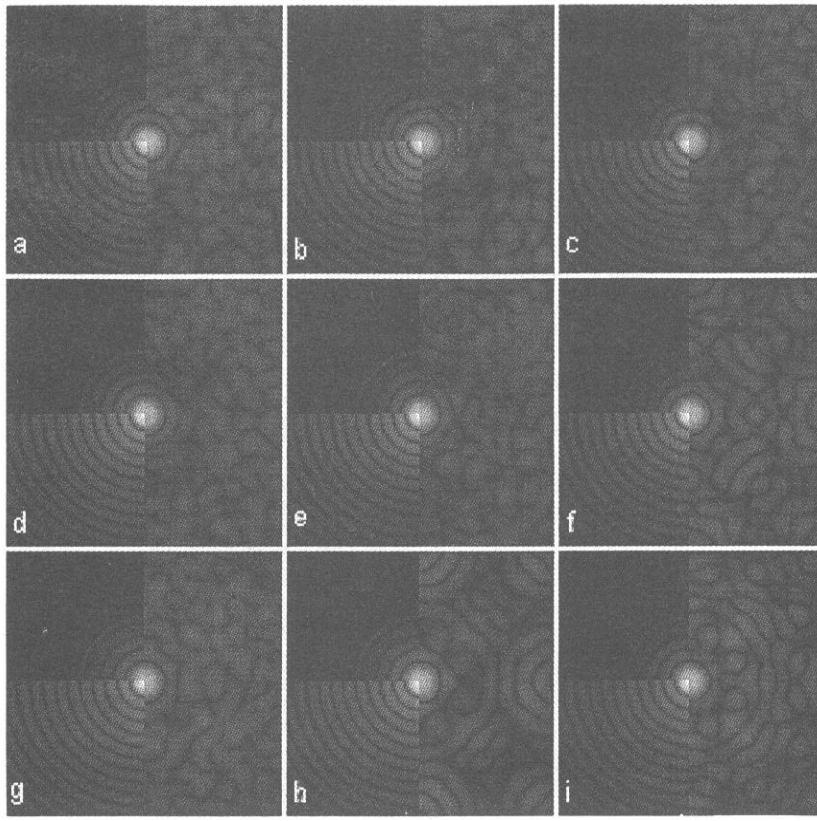

Figure 12. Squared moduli of the AIR of apodizing binary filters obtained with algorithms (a)–(i). In the upper left quadrants $|\text{AIR}|^2$ of the continuous-tone filter is shown. In order to demonstrate the apodizing properties of binary filters the $|\text{AIR}|^2$ of the clear pupil is shown in the lower left quadrants.

It is clear that all of the filters generated by the iterative Fourier transform algorithm are more efficient than the corresponding continuous-tone filters.

4. Discussion and conclusions

From the wide set of existing digital halftoning techniques, we have selected a subset of procedures (which belong to four different categories), which seemed well adapted for binarization of continuous-tone pupil filters. Furthermore, we have proposed two new algorithms as modifications of existing ones, to improve the performance of the original versions. Next, we have defined a merit function, the SNR, in order to evaluate the resemblance of the AIR of binary filters to the AIR of their continuous-tone counterpart. Then, after a numerical simulation, we have obtained the following results.

The resemblance between the spectrum of a binary pupil filter and that of its continuous-tone counterpart depends strongly on the binarization algorithm. In the case of sine-wave filters the SNR, which is the quantitative measure of this resemblance,

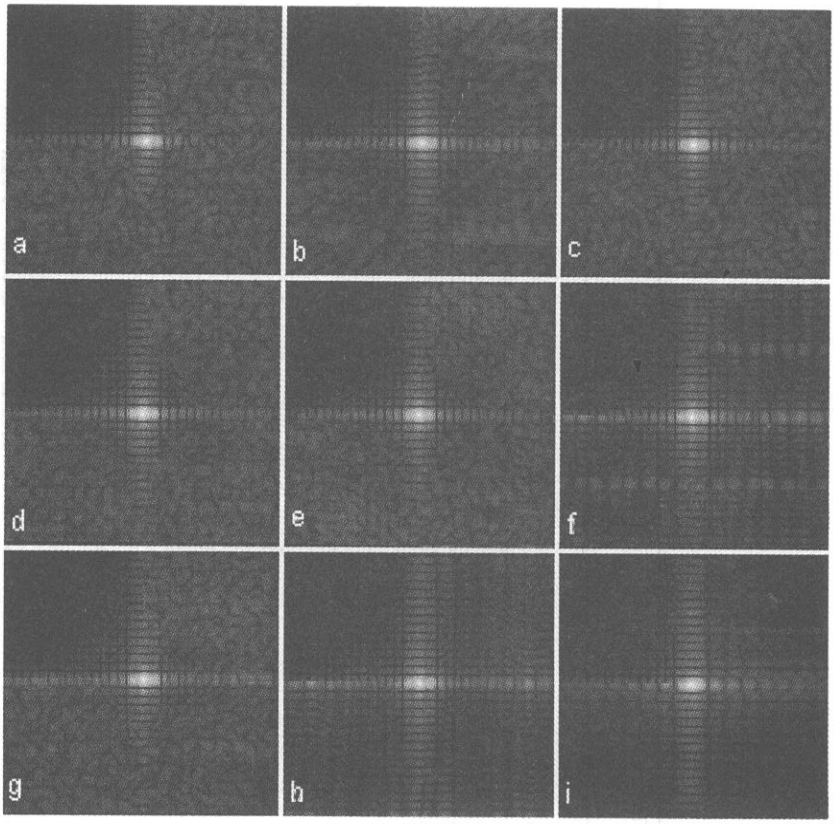

Figure 13. Squared moduli of the AIR of sine-wave filters obtained with algorithms (a)–(i). In the upper left quadrants the $|\text{AIR}|^2$ of the continuous-tone filter is shown.

varies within three orders of magnitude. The best resemblance is achieved for pupil filters generated with error diffusion algorithms. Among them, those which transfer the binarization error with random or randomly positioned weights provide the highest values of SNR. For rotationally symmetric filters the best binary realizations, chosen from an ensemble of 100 samples, were generated with only one randomly positioned weight (algorithm (c)). For the sine-wave pupil the best binary filter was generated with the Floyd–Steinberg error filter perturbed by a uniformly distributed bipolar additive noise (algorithm (d)).

The results obtained for the sine-wave pupil show that for continuous-tone filters that demonstrate a certain directionality, the SNR of binary filters generated by means of sequentially processed algorithms may be affected by the direction of processing. The classical Floyd–Steinberg algorithm (b) was found to be the only method that belonged to this class and yielded a rotation-invariant SNR. This may be related to the nearly isotropic spectrum of the binarization noise generated by the algorithm (b) (see figure 3 in [9]).

The question arises as to how to compare the results obtained with deterministic algorithms with those that use random number generators. Should we use in this comparison the SNR obtained for the best realization chosen from an ensemble or the

Table 2. Basic parameters of super-resolving (∪), apodizing (∩) and sine-wave (∩∪) filters generated with algorithms (a)–(i). The numbers in parentheses are obtained in the case when the corresponding algorithms are executed parallel to the ν axis (see equation (9c)). Other results correspond to the perpendicular direction of binarization.

	SNR			$\overline{\text{SNR}}$			σ_{SNR}			Relative light efficiency (α^{-1})		
Algorithm	∪	∩	∪∩	∪	∩	∪∩	∪	∩	∪∩	∪	∩	∪∩
(a)	949	6 806	4628	246	646	1105	150	776	755	0.797	0.943	1.102
(b)	1203	1 368	844 (808)	—	—	—	—	—	—	0.841	0.827	0.899 (0.898)
(c)	5775	23 024	10 062 (4663)	1756	3021	3444 (2854)	873	2927	1462 (577)	0.831	0.851	0.981 (0.987)
(d)	3429	1 635	4868 (34 522)	1708	784	2264 (17 647)	508	213	535 (3760)	0.831	0.834	0.975 (1.001)
(e)	4370	5 530	5577 (14 054)	1931	1507	2487 (9510)	570	745	658 (1707)	0.825	0.843	0.972 (0.999)
(f)	296	997	208	—	—	—	—	—	—	0.785	0.884	0.950
(g)	2287	1 113	293	528	345	288	293	143	22	0.851	0.862	0.968
(h)	1171	1 832	128	—	—	—	—	—	—	0.783	0.875	0.932
(i)	1420	19 578	36	—	—	—	—	—	—	1.165	1.052	1.294

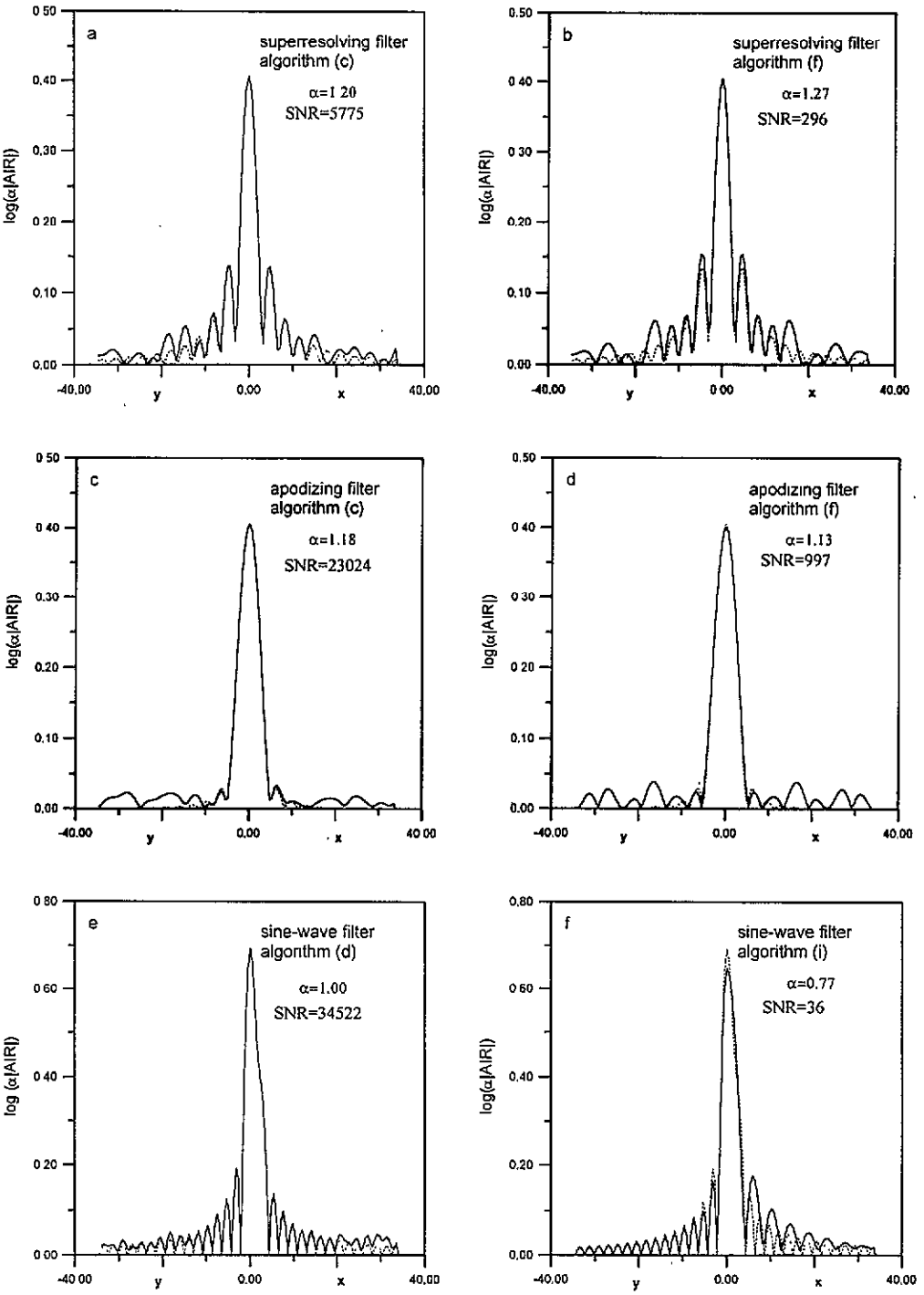

Figure 14. Cross sections of the intensity distribution in the image of the point source obtained with the best and the worst super-resolving, apodizing and sine-wave binary filters. The left- and the right-hand parts of the graphs represent the intensity distribution along semiaxes Oy and Ox, respectively. Dotted curves correspond to the AIR of continuous-tone filters.

average SNR? The $\overline{\text{SNR}}$ is more representative for a given binarization method than the SNR calculated for the best realization. On the other hand, those who seek the best binary representation of a continuous-tone filter usually accept the necessity to perform a numerical simulation in which a numerous set of realizations is generated to implement, finally, the best realization in a transmitting photosensitive material or in a computer-controlled spatial light modulator. We propose to rank the methods tested here according to another parameter which is a function of the highest SNR, $\overline{\text{SNR}}$ and σ_{SNR}, namely

$$\text{SNR}^*(N) = \overline{\text{SNR}} + \kappa(N)\sigma_{\text{SNR}} \tag{14}$$

where $\kappa(N)$ is the average derivation of the highest SNR from $\overline{\text{SNR}}$ in σ_{SNR} units and N is the number of sample filters in the ensemble. That is

$$\kappa(N) = \langle[\text{SNR}_{\max}(N) - \overline{\text{SNR}}]/\sigma_{\text{SNR}}\rangle \tag{15}$$

where $\langle\ \rangle$ denotes averaging over all ($\text{SNR}_{\max}$, $\overline{\text{SNR}}$, σ_{SNR}) obtained in numerical experiments which are performed in similar conditions. We assume that N is sufficiently large that $\overline{\text{SNR}}$ and σ_{SNR} are virtually independent of it. In our experiments $N = 100$, and the ratio of the size of the matrix of pixels used in the FFT to the size of filters is between 4 and 5. It is seen in table 2 that there are eighteen ($\text{SNR}_{\max}$, $\overline{\text{SNR}}$, σ_{SNR}) triplets.

Table 3. Ranking of binarization methods when SNR* is used as the merit function.

	algorithm	
	SNR*	
Super-resolving filter	Apodizing filter	Sine-wave filter
(c)	(i)	(d)
5775	19 578	34 943
(e)	(c)	(e)
4553	16 485	17 362
(d)	(e)	(c)
4045	4934	10 169
(g)	(a)	(a)
1875	4216	4578
(i)	(h)	(b)
1420	1832	844
(b)	(d)	(g)
1203	1763	364
(h)	(b)	(f)
1171	1368	208
(a)	(g)	(h)
936	1003	128
(f)	(f)	(i)
296	997	36

The averaging yields $\kappa(100) = 4.6$. This result means that it is quite common that in an ensemble of 100 sample filters generated in an experiment similar to ours the maximum SNR deviates from $\overline{\text{SNR}}$ by about $4.6\sigma_{\text{SNR}}$. We can say that SNR evaluates the performance of particular filters whereas SNR* evaluates halftoning methods. The ranking of methods based on the SNR* is presented in table 3. For deterministic algorithms we put SNR* = SNR. It can be seen that the results are somewhat object dependent, nevertheless they recommend the following algorithms (in this order): (c), (e), (d) and (i). When algorithms (c), (e) and (d) are used for binarization of filters that are not circularly symmetric it is worth trying various directions of processing. These three algorithms, the best from the point of view of the SNR*, belong, in fact, to the same class, i.e. error diffusion with random perturbations. This is because the error filter with one randomly positioned weight is equivalent to a two-weight filter whose weights are 100% perturbed. Namely, we have one pair of weights $(\frac{1}{2}, \frac{1}{2})$ which is perturbed as follows:

$$(\tfrac{1}{2}, \tfrac{1}{2}) \rightarrow (\tfrac{1}{2} + b\chi, \tfrac{1}{2} - b\chi). \tag{16}$$

In this case χ takes on with equal probability the values 0.5 and -0.5 whereas $b = 1$.

In the case of rotationally symmetric pupil filters, which is the case of considerable practical interest, our modifications ((e)) and (h)) resulted in higher values of both SNR and SNR* than the original versions ((d) and (f)). Thus the idea of employing hard clipped noise to perturbed the error weights (d) and to increase the number of testing points (h) seems justified.

The light efficiency of all the binary filters tested here is close to that of the corresponding continuous-tone filters. Therefore, it is reasonable to compare them on the basis of the SNR only. An evident trade-off between light efficiency and SNR demonstrates only the iterative Fourier transform algorithm (see the last row in table 2). Our results reveal another relation between α^{-1} and SNR: the higher the SNR the closer the light efficiency is to that of the continuous-tone filter. Both these relations can apply simultaneously only for superefficient filters ($\alpha^{-1} > 1$). This is exactly the case for the filters presented here which were generated with the iterative Fourier transform algorithm.

Acknowledgments

This work was partially supported by the Direccioń General de Investigacioń Científica y Tecnica (grant PB93-0354-602-01), Ministerio de Educacioń y Ciencia, Spain. MK carried out his research as part of the European Economic Community action Go West financed by the Commission of the European Communities under contract ERB-CIPA-CT-92-0135.

References

[1] Jaquinot P and Roizen-Dossier B 1964 *Progress in Optics* vol 3 ed E Wolf (Amsterdam: North-Holland)
[2] Hegedus Z S 1985 *Opt. Acta* **32** 815–26 and references therein
[3] Barnard T W 1971 *Appl. Opt.* **10** 2274–8
[4] Hegedus Z S 1990 *Confocal Microscopy* ed T Wilson (London: Academic) pp 171–83
[5] Ulichney R 1987 *Digital Halftoning* (Cambridge: MIT)
[6] Kermisch D and Roetling P G 1975 *J. Opt. Soc. Am.* **65** 716–23
[7] Broja M and Bryngdahl O 1993 *J. Opt. Soc. Am.* A **4** 554–60
[8] Pinhasi Y and Peri D 1993 *Opt. Commun.* **101** 277–85

[9] Weissbach S and Wyrowski F 1992 *Appl. Opt.* **31** 2518–34
[10] Mitsa T and Parker J 1992 *J. Opt. Soc. Am.* A **9** 1920–9
[11] Kowalczyk M, Andrés P and Martínez-Corral M 1992 *J. Opt. Soc. Am.* A **9** 1930–6
[12] Barnard E 1988 *J. Opt. Soc. Am.* A **5** 1803–17
[13] Billotet-Hoffman C and Bryngdahl O 1983 *Proc. Soc. Inf. Disp.* **24** 253–8
[14] Floyd R W and Steinberg L 1976 *Proc. Soc. Inf. Disp.* **17** 75–7
[15] Peli E 1991 *J. Opt. Soc. Am.* A **8** 625–36
[16] Broja M, Wyrowski F and Bryngdahl O 1989 *Opt. Commun.* **69** 205–10
[17] Peter T, Wyrowski F and Bryngdahl O 1993 *J. Mod. Opt.* **40** 591–600